PRECISION CRYOGENIC DILATOMETER FOR JAMES WEBB SPACE TELESCOPE MATERIALS TESTING[1]

Matthew J. Dudik[2], Peter G. Halverson, Marie Levine,

Martin Marcin, Robert D. Peters, Stuart Shaklan

NASA Jet Propulsion Laboratory

California Institute of Technology

4800 Oak Grove Drive

Pasadena, CA 91109

[1] Paper presented at the Fifteenth Symposium on Thermophysical Properties, June 22-27, 2003, Boulder, Colorado, U.S.A.

[2] To whom correspondence should be addressed. Email: matthew.j.dudik@jpl.nasa.gov

ABSTRACT

The James Webb Space Telescope (JWST) will be a 6 meter diameter segmented reflector. It will be launched at room temperature, but will be passively cooled to 30 to 40 Kelvin when it reaches its planned location at the L2 point.

Because of the 270 Kelvin drop in temperature after launch, understanding the thermophysical properties of mirror, secondary optics, and supporting structures is crucial to the design of an instrument that will provide diffraction limited performance at 2 microns. Once deployed, JWST will perform continuous science for durations ranging from one day to a month, hence an understanding of how small temperature fluctuations will impact the nanometric stability of the optical system through thermal expansion is required.

The JWST materials testing team has designed and built a novel cryogenic dilatometer based on the <100 pm technology previously developed for the Space Interferometry Mission. Samples will be tested in a cryo-cooled vacuum environment with temperature monitored to <10 mK. Our goal is coefficient of thermal expansion (CTE) measurements accurate to 1ppb/K for copper (for intercomparison with other laboratories) and ~ 0.1 ppb/K for ULE, for a nominal CTE = 30ppb/K. The dilatometer will be used to measure the CTE of samples from JWST primary mirror prototypes, local CTE variations from multiple locations on a prototype mirror, CTE variations from batch to batch of the same material, and thermal and mechanical creep measurements from room temperature down to 30 K.

KEY WORDS: coefficient of thermal expansion, cryogenic, dilatometer, strain

INTRODUCTION

The James Webb Space Telescope (JWST) is a 6-meter class infrared space telescope that will have a primary mirror wave-front error (WFE) of 60 nm and will be passively cooled to 30 to 40 Kelvin. In order to adequately design the telescope, improved knowledge of the thermophysical properties of various low expansion materials is necessary. Specifically, knowledge of the mirror and back structure material's coefficient of thermal expansion (CTE) as well as CTE homogeneity are of critical importance since they can lead to large thermal stresses and/or misalignment of optical components. Finite element analysis of JWST's primary mirror indicated that, in order to maintain a WFE of 60 nm, the CTEs of the back structure (composite) and mirror substrate (ULE or Be O-30) must be understood to a level less than 10 ppb/K down to 30 K. In order to meet these needs, a novel cryogenic dilatometer has been developed by the JWST materials testing team. The dilatometer has been designed to eliminate back-out factors and minimize systematic errors by implementing a non-contact length determination technique that uses an interferometer whose long-term stability is defined by a stabilized laser. An ULE sample from the JWST Advanced Mirror System Demonstrator (AMSD) optics has been tested over the temperature range of 300 to 30 K in order to demonstrate the dilatometer's capabilities. System calibration activities are in progress and measurements of standard samples for intercomparison with other laboratories are planned.

APPARATUS

The JPL cryogenic dilatometer is comprised of a laser source, heterodyne interferometer, cryogenically cooled sample, sample alignment stage, and data acquisition and control system. A diagram and photo of the cryogenic dilatometer are given in Figure 1 and 2, respectively.

Laser Source. The laser source is similar to that described by *Zhao et al.*[1] and consists of a temperature stabilized, monolithic, non-planar ring oscillator (NPRO) 100 mW doubled YAG laser at $\lambda = 532$ nm, two RF driven acousto-optic modulators (AOMs), various optics/ beamsplitters, and fiber couplers. The AOMs shift the frequency of the local oscillator beam by 80 MHz and the measurement beam by 80.016 MHz resulting in a heterodyne beat frequency of 16 kHz. The beams are coupled into two angle polished, polarization-maintaining fibers in a vacuum feed-through. The angle polished ends of the fibers minimizes back reflections while the vacuum feed-through allows the transfer of light through the vacuum chamber wall without the use of a window. Thus, mixing of back-scattered light with incoming light is minimized and the thermal gradient effect of a window is eliminated.

Interferometer. The interferometer is a differential, heterodyne interferometer. Its optical layout is similar to that described by Zhao *et al*.[2] and consists of a monolithic interferometer baseplate, six Zerodur bipods, two Zerodur off-axis parabolic mirrors (OAP), two beam masks, two beam dumps, two beamsplitters, and a detector board. All components are mounted symmetrically about the center of the baseplate to minimize bending and de-centering errors while the baseplate is held by 3 Zerodur bipods to minimize lateral motion errors. Light from the local oscillator and measurement fibers are coupled to the baseplate and collimated by two Zerodur OAPs. The OAPs are held by flexural invar mounts whose position relative to the baseplate is fixed by three zerodur bipods. As a result, the OAPs are kinematically held at their 63 cm focal lengths by low expansion materials that minimize defocus error while collimating the beams into two 5 cm diameter beams. Both beams are directed downward toward the interferometer baseplate such that the two beams pass through beam masks. The local oscillator mask trims the Gaussian edge of the collimated beam to 5 cm in diameter while the measurement

beam mask splits the collimated beam into three 3 mm reference beams (clocked 120˚ from one another) and a 3 mm test beam in the center. Both the local oscillator beams and four measurement beams pass through separate 50% transmitting beamsplitters, 0.5˚ wedged to reject ghost reflections. The measurement beams are reflected off the object of interest, directed back towards the interferometer where they mix with the local oscillator beam, and illuminate an array of photodetectors arranged in the same pattern as the measurement beam mask. The remaining light reflected by the splitters is sent to beam dumps mounted to both sides of the interferometer baseplate. Since both the reference and test beams follow the same path, many error sources, such as temperature induced changes in beamsplitter thickness, fiber optic phase delays, relaxation of optical mounts, are common mode and do not effect the final measurement[3].

Sample. The sample consists of a pillar optically contacted to a base of the same material. The pillar and base are fabricated to optical quality ($\lambda/4$ wave peak-to-valley flatness, < 9 arcsecs parallelism, 60-40 scratch-dig) to provide parallel reflecting surfaces. The sample surfaces are not coated with a reflective material and are of the same material to eliminate bimetallic bending and surface distortions due to CTE mismatches. Additionally, the sample base sides and back surface are not polished to minimize ghost reflections. The sample base is kinematically mounted in a cryogenic dewar by three bipods that thermally couple the sample to the dewar without introducing large bending stresses.

Cryogenic Environment. The sample is cooled by a cryogenic system consisting of an aluminum dewar, heaters, heat transfer line, and a closed cycle cryostat. The cylindrical dewar is constructed of a thick Al 6061 base, sides, and top which is coupled to the cryostat via oxygen-free copper braids which provide conductive heat transfer while minimizing the transfer of vibrations to the dewar. Holes have been machined in the top of the dewar in the layout of the

measurement beams to allow the beams to pass through the top unobstructed. Multi-layer insulation (MLI) provides a radiation shield for the dewar, heat transfer line, and cryostat in order to minimize heat loss. The dewar is kinematically mounted to an alignment stage by three Zerodur bipods to minimize heat loss while minimizing beam walk errors.

Alignment Stage. The alignment stage is a piezoelectric driven, athermal, monolithic, flexure tip/ tilt stage. The kinematic stage consists of three piezoelectric actuators (pzts), three invar "rough" alignment screws, invar spherical-ended nuts, and a monolithic invar tip/ tilt flexure casing. Rough tip/ tilt adjustments are made by increasing (decreasing) the length of the invar screw by moving the spherical-ended nuts along the screw. The increase (decrease) of the screw pushes (pulls) on a flexural tangent bar on the monolithic stage resulting in a tip/ tilt of the stage up to 23 milliradians with resolution better than 13 microradians. Further tip/ tilt adjustments of the stage are accommodated via piezoelectric stacks. As with the rough adjustments, the pzt actuators push on a flexure tangent bar resulting in adjustment capability of 220 microradians with resolution to better than 0.15 nanoradians. Due to the negative thermal expansion of the pzt stacks and low expansion of the monolithic flexural invar housing, the stage is athermalized for a typical thermal gradient of 100 mK. Since all adjustments are symmetric and kinematic, any tip/ tilt adjustment of the stage is made about its center.

Data Acquisition and Control. The data acquisition and control system is a LabView driven, PC based system consisting of a phase measuring system, active tip/ tilt alignment feedback control, and active thermal monitoring and control system. The picometer class phase measuring system consists of a photodiode and pre-amp board, zero-crossing detector, and phasemeter previously developed at JPL for the Space Interferometry Mission (SIM)[4]. The detector board consists of pre-amps and photodiodes arranged in the same pattern as the beam

mask on the interferometer. When interfering light from the measurement and local oscillator beams are shone on their diodes, nominal 16 kHz heterodyne signals are produced which are amplified, filtered, and converted into square waves whose relative phases are measured and recorded.

An active tip/ tilt alignment feedback control is used to maintain precision alignment of the object of interest relative to the interferometer. The LabView driven control equalizes the optical paths of the interferometer's reference beams resulting in an active precision alignment of the sample base relative to the interferometer.

Temperature monitoring and control of the cryogenic system and sample are achieved through the use of a Lakeshore 340, multiplexer, and silicon diodes. The Lakeshore 340 measures and controls the cryogenic system and sample's temperature and cycling rate. Silicon diodes are attached to the cryogenic system and sample in order to determine their temperatures and thermal gradients. Since the Lakeshore sensor input is limited to four sensors, a multiplexer was added to increase that number to eleven.

MEASUREMENT PROTOCOL

A 6 mm thick, 7 mm wide, 25 mm long ULE sample pillar is optically contacted to a 38 mm diameter, 13 mm thick ULE sample base cut from the same mirror substrate. Three temperature sensors are bonded to the sample base clocked 120˚ from one another and two sensors are attached to the sample pillar in order to measure the sample's temperature and thermal gradients. The sample is mounted to the cryogenic dewar that is housed inside the 61cm diameter bell jar type vacuum chamber. After installing the dewar sides, top, and MLI, the sample is aligned to the interferometer via the alignment stage and a 10^{-6} Torr vacuum is

achieved. Thermal loads are applied to the sample in temperature decrements of 20 K from room temperature. The sample is allowed to soak at each temperature set point until the diodes register a temperature stability of better than 10 mK for ~ twenty minutes. The thermal expansion (contraction) of the sample pillar is measured relative to its base by determining the phase difference between the interferometer's test and reference beams that reflect from the pillar and base, respectively. As the sample pillar expands (contracts) with the thermal loads, the test beam's heterodyne phase increases (decreases) relative to the average of three reference beams phases indicating a relative expansion (contraction) of the sample pillar. The differential phase measurements are converted to relative length measurements of the sample pillar and recorded with the temperature data via a PC. The thermal strain ($\sigma_{THERMAL}$) is calculated by dividing the thermal expansion (contraction) measurements by the sample's absolute length at 293 K, L_0 (typically = 24 mm). The corresponding local coefficient of thermal expansion (α) is then determined by dividing the thermal strain by the temperature load (ΔT) according to the equation $\alpha = (\sigma_{THERMAL})(\Delta T)^{-1}$.

ERROR ALLOCATION AND SYSTEM CALIBRATION

An error budget (Figure 3) was developed in order to determine the cryogenic dilatometer's ULE thermal strain and CTE measurement resolutions. The errors are compiled into three groups consisting of relative length measurement errors ($d(\Delta L)$), absolute length measurement errors ($d(L)$), and temperature monitoring errors ($d(\Delta T)$) according to the CTE measurement error ($d\alpha$) equation:

$$\frac{d\alpha}{\alpha} = \sqrt{\left(\frac{d(\Delta L)}{\Delta L}\right)^2 + \left(\frac{d(L)}{L}\right)^2 + \left(\frac{d(\Delta T)}{\Delta T}\right)^2}$$

Among the errors listed, typical measurement precision limiting factors include the system thermo-optic error, frequency stability, and periodic nonlinearity (cyclic error). The thermo-optic error is a measure of the dilatometer's thermal stability as the interferometer is pointed at a flat, low expansion mirror (i.e. sample base). The frequency stability is a measure of the system's frequency drift of the laser source over non-common path segments of an interferometer due to the sample pillar length. Lastly, the periodic nonlinearity is a measure of the dilatometer's ability to measure a pure piston motion.

Calibration of the thermo-optic error, frequency stability, and periodic nonlinearity measurement details are as follows. The thermo-optic error is measured by reflecting the four sample measurement beams off the ULE sample base while maintaining the temperature of the base at 300 K +/- 5 mK. The frequency stability is measured by optically contacting the sample pillar to the its base and reflecting the measurement beams off the ULE sample base and pillar while maintaining the same temperature requirements as in the thermo-optic calibration. The periodic nonlinearity of the system is measured by blocking the beams at the beam mask, one at a time, and measuring signal leakage as described by Halverson *et al.*[5].

RESULTS AND DISCUSSIONS

Calibration Results. Results of the thermo-optic calibration run are given in Figure 4 (some of the values have been offset such that all plots fit on one graph). From examination of the various plots, we observe a piston measurement error drift of ~ 700 pm peak-to-peak (P-P) or 167 pm root mean square (RMS) over 12 hrs that is independent of the 15 mK temperature stability of the sample, is correlated with the 1.6 K thermal drift of the post-amp board's temperature, and follows the laser cooling block's 650 mK temperature drift. As a result, the

thermo-optic performance could likely be improved by stabilizing the temperature of the post-amp board and the laser's cooling block.

The result of the frequency stability calibration run revealed an error of ~ 757 pm P-P or 180 pm RMS over 8hrs (some of the values have been offset such that all plots fit on one graph). From examination of Figure 5, the ~ 11 MHz frequency drift of the laser source is independent of the sample pillar's 9 mK temperature stability, lags the 1.4 K thermal drift of the post-amp board, and is correlated with the 310 mK thermal stability of the laser's cooling block. As observed in the thermo-optic calibration run, the frequency stability could likely be improved by stabilizing the temperature of both the laser source and post-amp boards. Also, locking of the laser's frequency to an iodine line will minimize the effect of the non-common path error due to the sample pillar height.

Lastly, the periodic nonlinearity calibration revealed errors of 30 pm for channel 0 (test beam reflected off the sample pillar) and 50, 94, and 31 pm for channels 1, 2, and 3, respectively (three reference beams reflected off the sample base). The total system periodic nonlinearity of 115 pm RMS is dominated by the error in channel 2. This may be due to light reflecting and/ or diffracting off the photodiode casing, electrical crosstalk, optical crosstalk due to stray light from another beam, etc. Further experimentation is necessary to determine the various contributors.

Thermal Strain and CTE Results. Figure 6 shows thermal strain measurements of ULE which were obtained using the data that met the 10 mK stability requirement for each 20 K temperature plateau. The results show that the ULE sample contracts by 0.86 ppm from 300 to 260 K and then expands by ~117 ppm when cooled from 260 to 30 K. Additionally, the results show that the coefficient of thermal expansion decreases from .039 to –0.9 ppm/K from 300 to

50K and then begins to increase to -.88 ppm/K at 35 K. The room temperature results are consistent with those given by Pacquin[6] who states that the CTE of ULE is .03 +/- .015 ppm/K.

The strain and temperature standard deviations are given in Figure 7 for each 20 K plateau. All strain measurements were obtained while the sample temperature was stable to within 10 mK. The plot shows strain standard deviations less than 35 ppb for temperatures above 100 K and deviations less than 85 ppb for all other temperature plateaus. The 35 ppb measurement scatter correlates well with the dilatometer's measurement resolution of 33 ppb as given by the error budget when the material is still a low expansion material. For the remaining temperatures plateaus below 150 K, the strain standard deviation was less than 83 ppb. This higher standard deviation may be due to drift in electronics, pointing instability, vibrations, thermal sensor errors due to mounting stresses, etc. Further investigation is required.

Lastly, a 3.35 nm P-P or 800 pm RMS oscillation in the test beam was observed during the 20 K temperature ramps and decreases to ~ 335 pm P-P or 80 pm RMS when the temperature of the sample is stabilized to within 10 mK. The oscillations are likely due to an imperfect optical contact between the sample base and pillar. As the sample temperature varies, its index of refraction varies causing variations in the path length through the sample. If the sample pillar is not fully contacted to the base, then back reflections from the sample pillar's contacting face will mix with the reflected beam from the pillar top resulting in a piston measurement that includes the true pillar thermal expansion plus changes in the path length due to variations in the pillar's index of refraction. As such, the contacting error may be minimized by better surface preparation prior to contacting the sample pillar to its base. Further investigation is necessary to adequately understand this behavior.

SUMMARY AND CONCLUSIONS

A novel cryogenic dilatometer has been developed to eliminate back out factors and minimize system errors in order to provide high precision coefficient of thermal expansion measurements from 310 to 30 Kelvin. Initial calibrations of the system including thermo-optic, frequency stability, and periodic nonlinearity were performed in order to characterize the system errors. Results of the calibration runs indicate that the temperature drift of the laser's cooling block and post-amp boards as well as imperfect sample contacting currently limit the cryogenic dilatometer's measurement precision to 33 ppb. As such, the cryogenic dilatometer's CTE measurement precision of ULE is currently ~1.7 ppb/K for a 20 K thermal load or 0.12 ppb/K for a 280 K thermal load. ULE's CTE was measured over the temperature range of 300 to 30 K. The resulting room temperature CTE of .039 ppb/K correlates well with existing knowledge of ULE's CTE.

Upgrades to this facility are currently being undertaken and include an iodine cell to improve the laser source's frequency stability, development of a measurement jig to calibrate the system's periodic nonlinearity, and temperature controlled post-amp boards to minimize long-term thermal drift. Future experiments include repeating the frequency stability, periodic nonlinearity, and thermo-optic tests upon installation of upgraded components as well as inter-comparisons of standard samples with other laboratories.

ACKNOWLEDGEMENTS

The authors would like to thank Don Moore, Feng Zhao, and R. Scott Leland for their insights and many contributions. We also gratefully acknowledge the generous support of NASA's James Webb Space Telescope project for funding this facility.

REFERENCES

1. F. Zhao, J. Logan, S. Shaklan, M. Shao, SPIE Proceedings of Optical Engineering for Sensing and Nanotechnology, **3740**:642 (1999).
2. F. Zhao, Proceeding of the ASPE Annual Meeting, 345 (2001).
3. F. Zhao, R. Diaz, P. Halverson, G. Kuan, S. Shaklan. Proceedings of Optoelectronic Distance Measurement and Applications, 39 (2001).
4. P. Halverson, D. Johnson, A. Kuhnert, S. Shaklan, R. Spero, SPIE Proceedings of Optical Engineering for Sensing and Nanotechnology, **3740**:646 (1999).
5. P. Halverson, R. Spero, J. Opt. A, **Pure Appl. Opt. 4**:S304 (2002).
6. R. Pacquin, SPIE Shortcourse on Materials for Precision Instruments, **SC016**:39 (2002).

FIGURE CAPTIONS

Fig. 1. Schematic of the cryogenic dilatometer.

Fig. 2. Photograph of the cryogenic dilatometer.

Fig. 3. Cryogenic dilatometer error budget.

Fig. 4. Results of the thermo-optic calibration test.

Fig. 5. Results of the frequency stability calibration test.

Fig. 6. ULE thermal strain and coefficient of thermal expansion as a function of temperature.

Fig. 7. Thermal strain and temperature standard deviations as a function of sample temperature.

Fig. 8. Sample pillar de-contacting and temperature as a function of time.

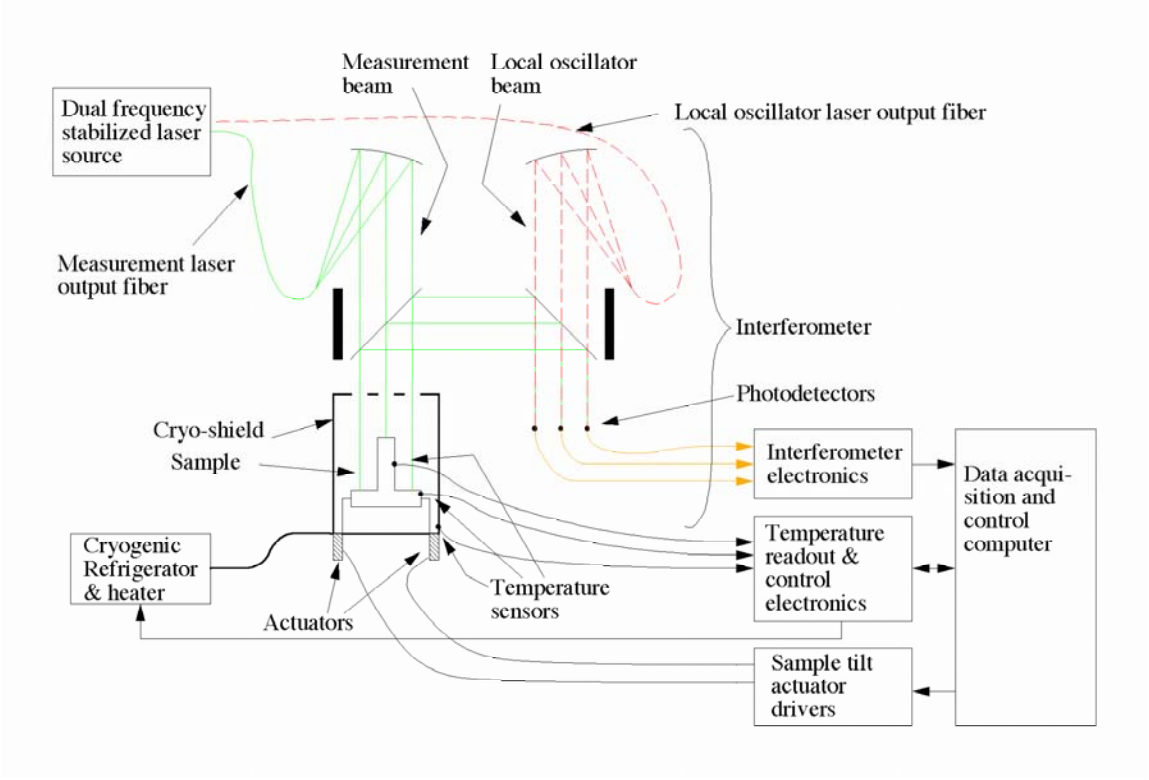
Measurement beam
Local oscillator beam
Dual frequency stabilized laser source
Local oscillator laser output fiber
Measurement laser output fiber
Interferometer
Photodetectors
Cryo-shield
Sample
Interferometer electronics
Data acquisition and control computer
Temperature readout & control electronics
Cryogenic Refrigerator & heater
Temperature sensors
Actuators
Sample tilt actuator drivers

Fig. 1

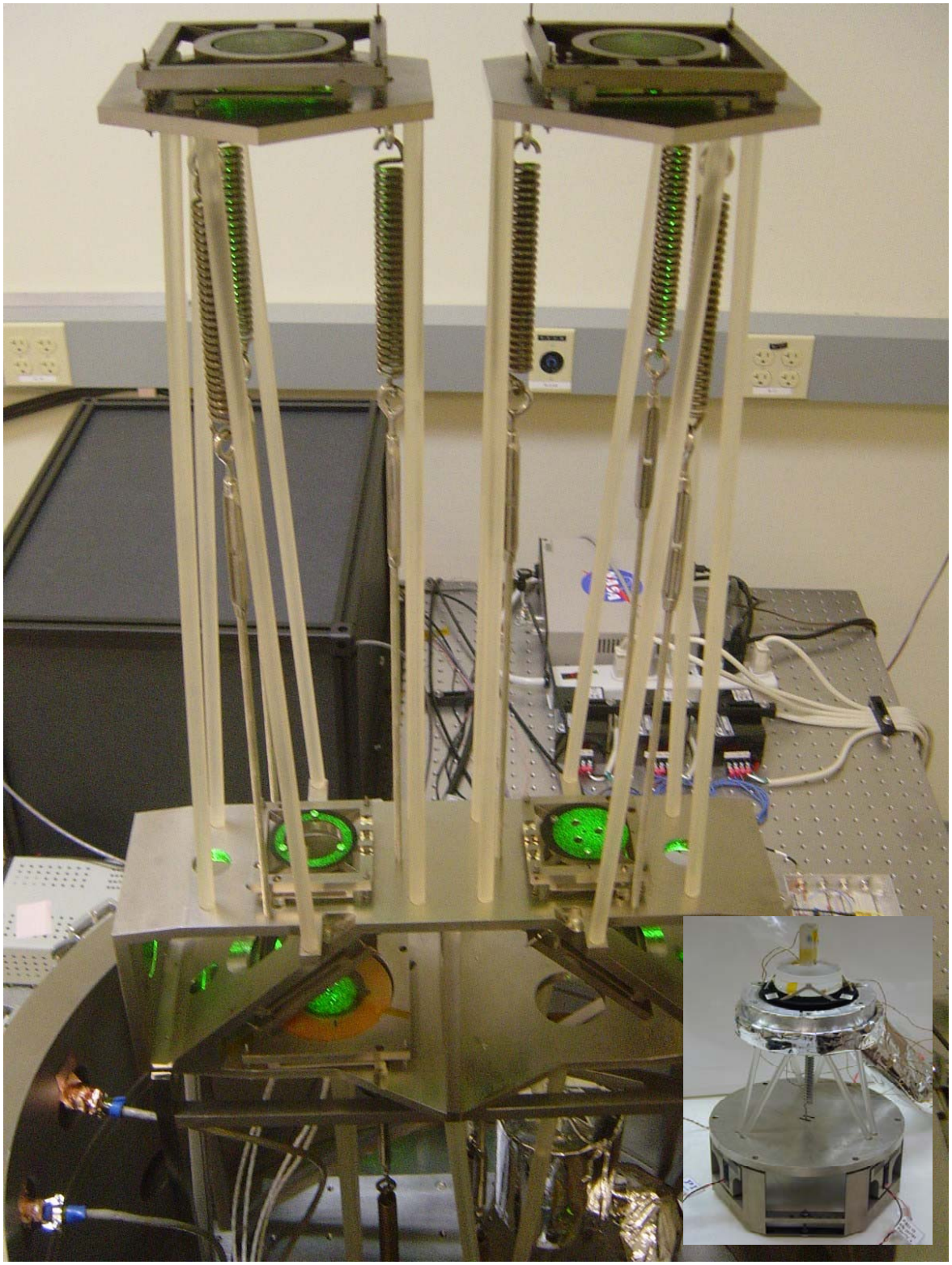

Fig. 2

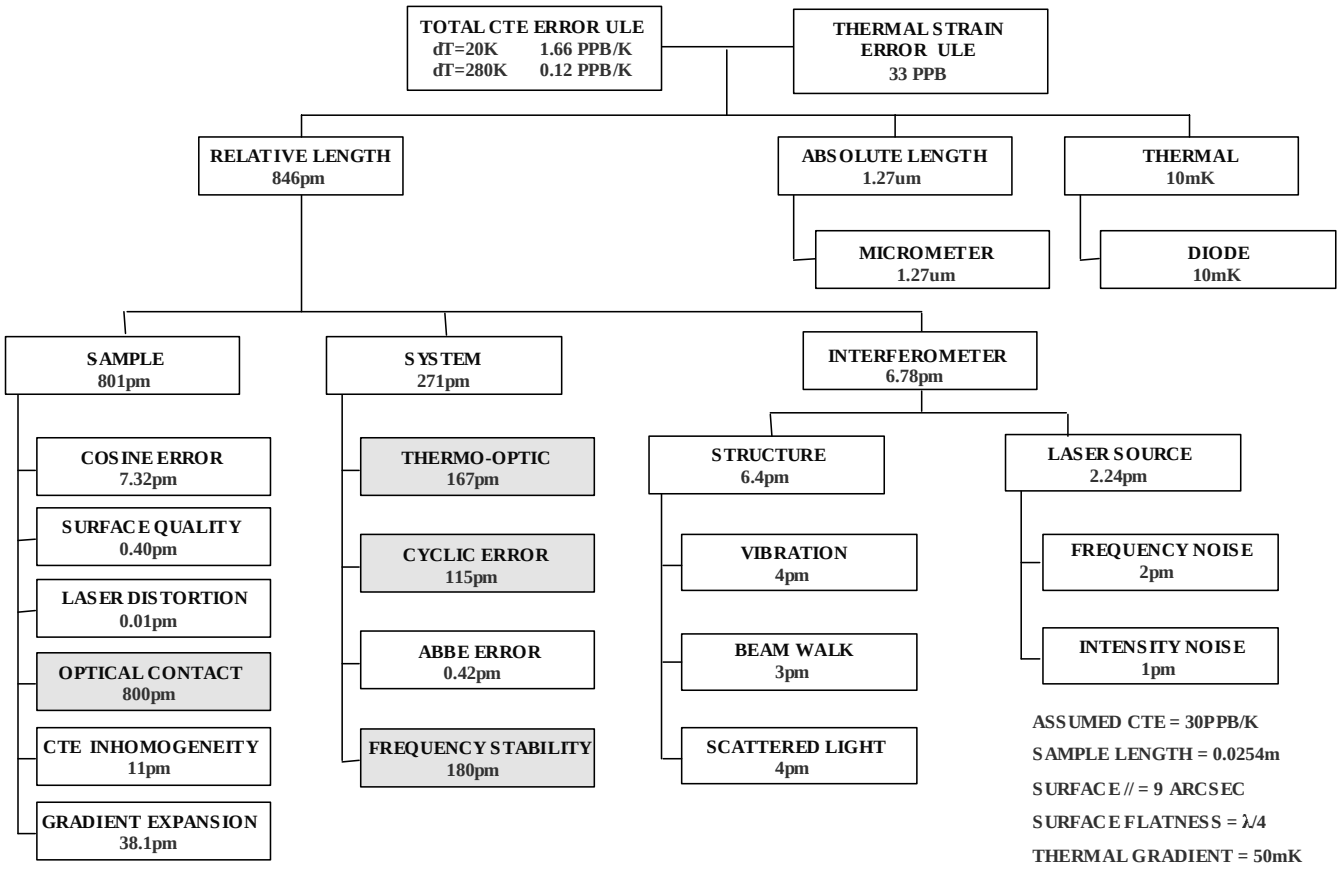
TOTAL CTE ERROR ULE
dT=20K 1.66 PPB/K
dT=280K 0.12 PPB/K
THERMAL STRAIN ERROR ULE
33 PPB
RELATIVE LENGTH
846pm
ABSOLUTE LENGTH
1.27um
THERMAL
10mK
MICROMETER
1.27um
DIODE
10mK
SAMPLE
801pm
SYSTEM
271pm
INTERFEROMETER
6.78pm
COSINE ERROR
7.32pm
SURFACE QUALITY
0.40pm
LASER DISTORTION
0.01pm
OPTICAL CONTACT
800pm
CTE INHOMOGENEITY
11pm
GRADIENT EXPANSION
38.1pm
THERMO-OPTIC
167pm
CYCLIC ERROR
115pm
ABBE ERROR
0.42pm
FREQUENCY STABILITY
180pm
STRUCTURE
6.4pm
LASER SOURCE
2.24pm
VIBRATION
4pm
BEAM WALK
3pm
SCATTERED LIGHT
4pm
FREQUENCY NOISE
2pm
INTENSITY NOISE
1pm
ASSUMED CTE = 30PPB/K
SAMPLE LENGTH = 0.0254m
SURFACE // = 9 ARCSEC
SURFACE FLATNESS = λ/4
THERMAL GRADIENT = 50mK

Fig. 3

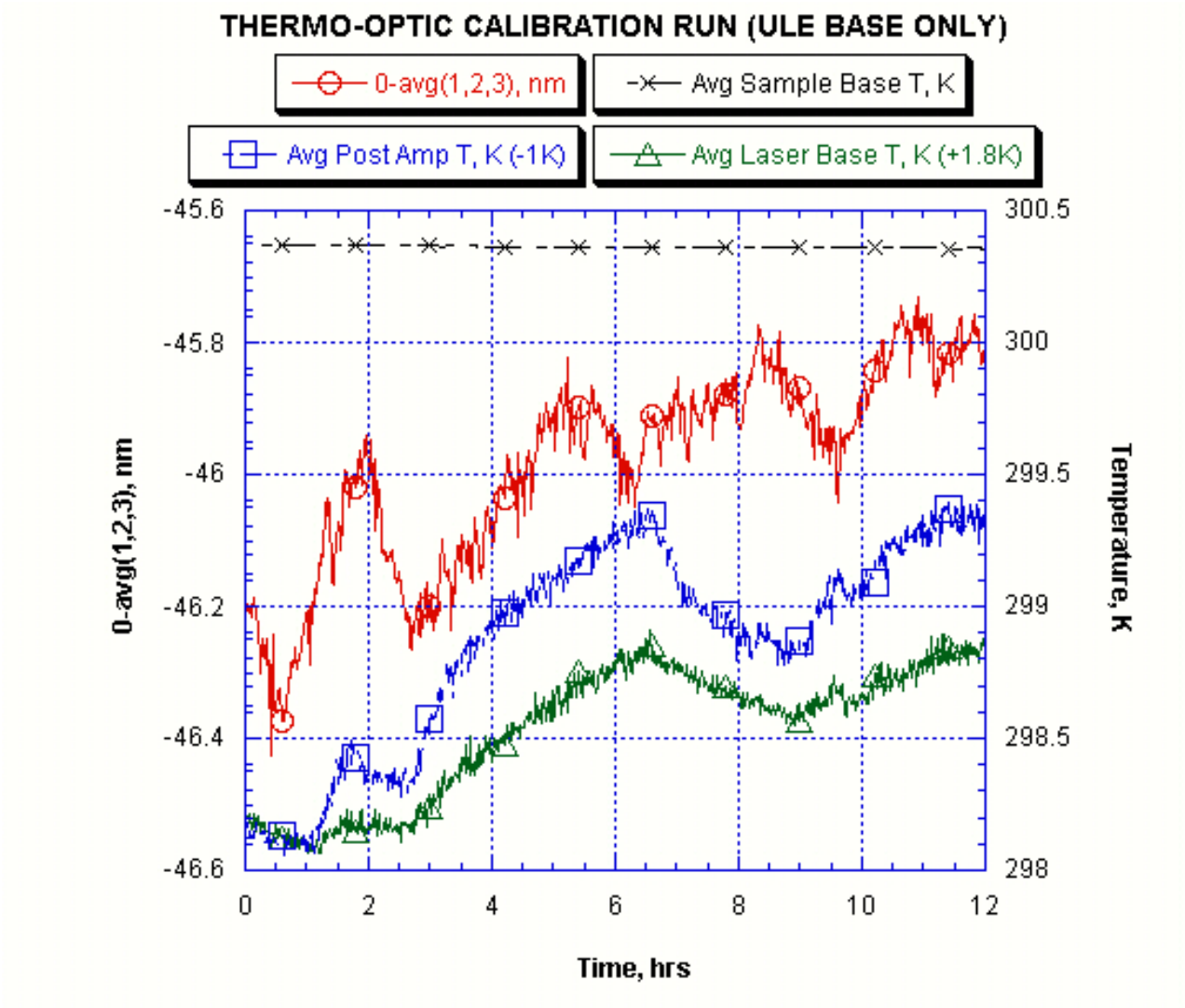
THERMO-OPTIC CALIBRATION RUN (ULE BASE ONLY)
0-avg(1,2,3), nm
Avg Sample Base T, K
Avg Post Amp T, K (-1K)
Avg Laser Base T, K (+1.8K)
-45.6
-45.8
-46
-46.2
-46.4
-46.6
0-avg(1,2,3), nm
300.5
300
299.5
299
298.5
298
Temperature, K
0
2
4
6
8
10
12
Time, hrs

Fig. 4

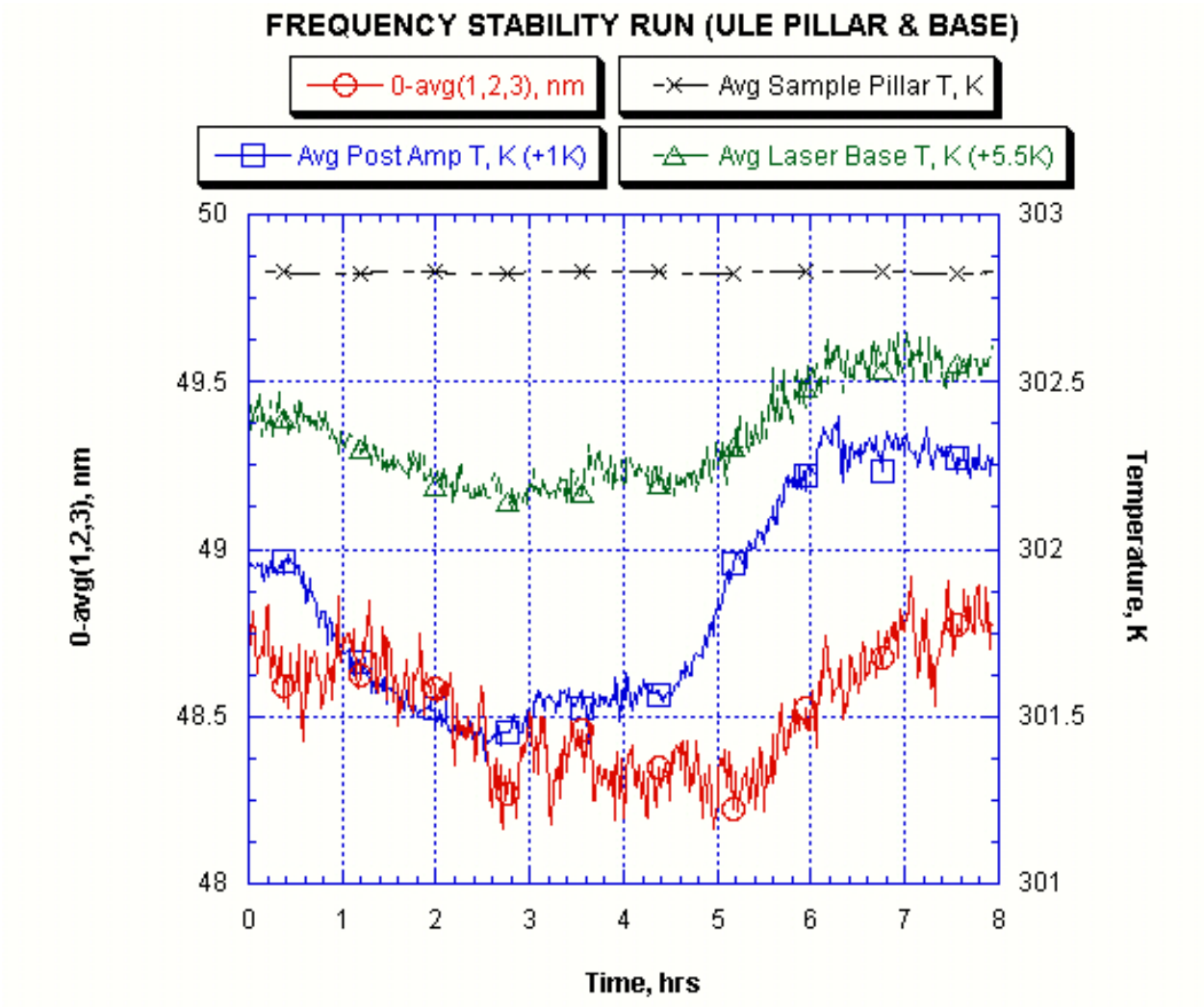
FREQUENCY STABILITY RUN (ULE PILLAR & BASE)
0-avg(1,2,3), nm
Avg Sample Pillar T, K
Avg Post Amp T, K (+1K)
Avg Laser Base T, K (+5.5K)
50
49.5
49
48.5
48
303
302.5
302
301.5
301
0
1
2
3
4
5
6
7
8
0-avg(1,2,3), nm
Temperature, K
Time, hrs

Fig. 5

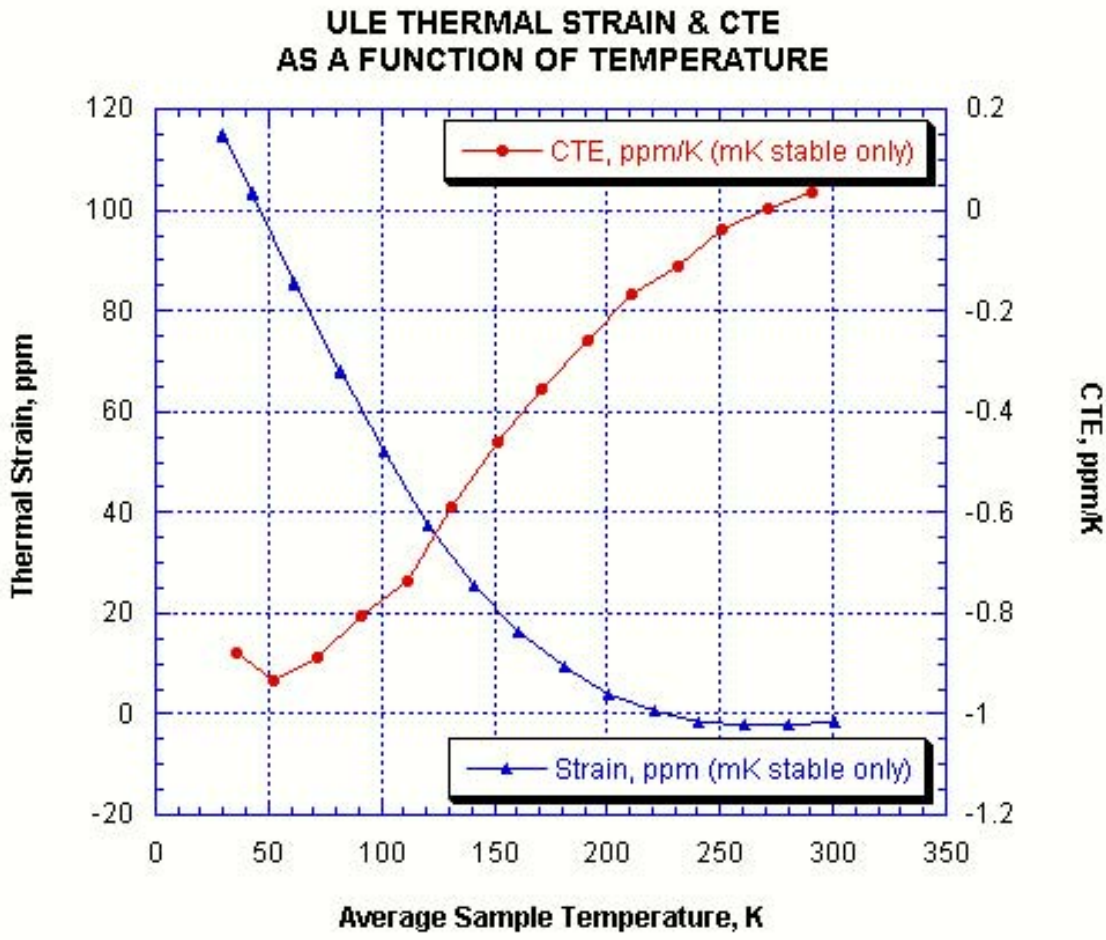
ULE THERMAL STRAIN & CTE
AS A FUNCTION OF TEMPERATURE
Thermal Strain, ppm
CTE, ppm/K
Average Sample Temperature, K
CTE, ppm/K (mK stable only)
Strain, ppm (mK stable only)
120
100
80
60
40
20
0
-20
0.2
0
-0.2
-0.4
-0.6
-0.8
-1
-1.2
0
50
100
150
200
250
300
350

Fig. 6

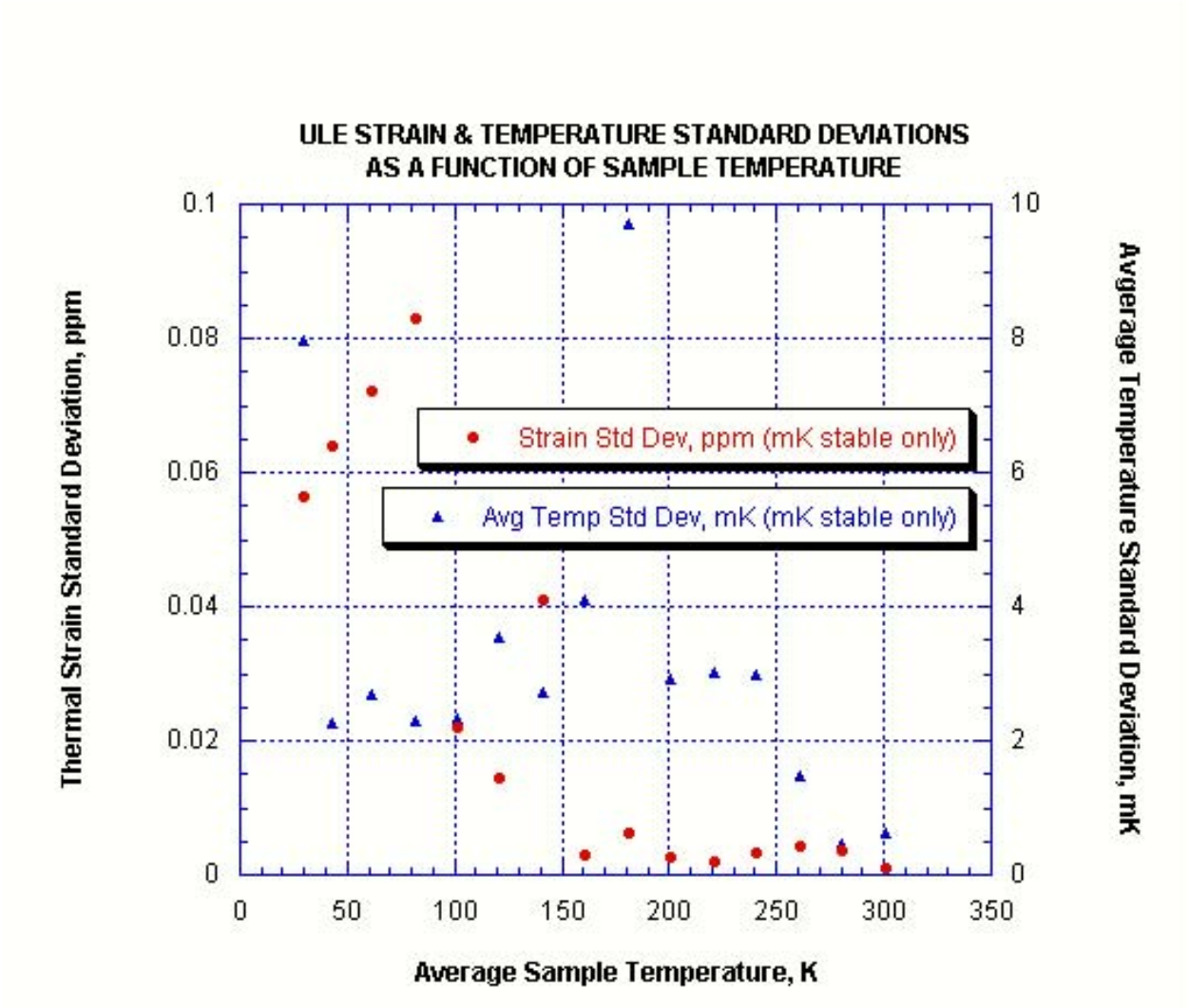
ULE STRAIN & TEMPERATURE STANDARD DEVIATIONS
AS A FUNCTION OF SAMPLE TEMPERATURE
Thermal Strain Standard Deviation, ppm
Avgerage Temperature Standard Deviation, mK
Average Sample Temperature, K
Strain Std Dev, ppm (mK stable only)
Avg Temp Std Dev, mK (mK stable only)
0.1
0.08
0.06
0.04
0.02
0
10
8
6
4
2
0
0
50
100
150
200
250
300
350

Fig. 7

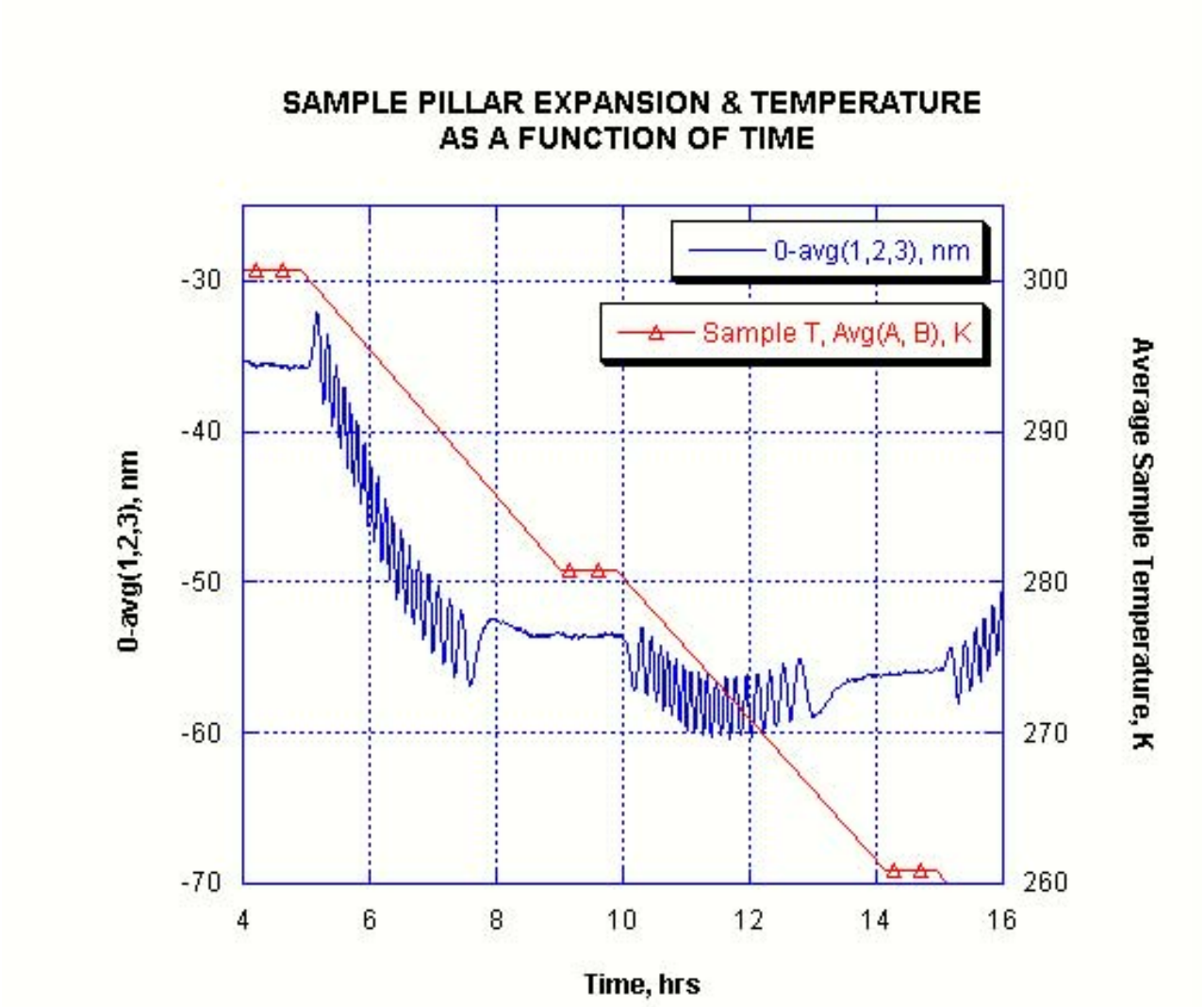
SAMPLE PILLAR EXPANSION & TEMPERATURE
AS A FUNCTION OF TIME
0-avg(1,2,3), nm
Sample T, Avg(A, B), K
-30
-40
-50
-60
-70
300
290
280
270
260
4
6
8
10
12
14
16
0-avg(1,2,3), nm
Average Sample Temperature, K
Time, hrs

Fig. 8